

Resilience of helical fields to turbulent diffusion II: direct numerical simulations

Pallavi Bhat^{1*}, Eric G. Blackman^{2†} and Kandaswamy Subramanian^{1‡}

¹*IUCAA, Post Bag 4, Ganeshkhind, Pune 411007, India.*

²*Department of Physics and Astronomy, University of Rochester, Rochester, NY14618, USA*

10 August 2021

ABSTRACT

The recent study of Blackman and Subramanian (Paper I) indicates that large scale helical magnetic fields are resilient to turbulent diffusion in the sense that helical fields stronger than a critical value, decay on slow (resistively mediated), rather than fast (\sim turbulent) time scales. This gives more credence to potential fossil field origin models of the magnetic fields in stars, galaxies and compact objects. Here we analyze a suite of direct numerical simulations (DNS) of decaying large scale helical magnetic fields in the presence of non-helical turbulence to further study the physics of helical field decay. We study two separate cases: (1) the initial field is large enough to decay resistively, is tracked until it transitions to decay fast, and the critical large scale helical field at that transition is sought; (2) the case of Paper I, wherein there is a critical initial helical field strength below which the field undergoes fast decay right from the beginning. For case (1), the initial decay rate in the slow regime is on an average about twice that of a purely resistive decay and both simulations and solutions of the two scale model (from Paper 1), reveal that the transition energy, E_{c1} , is independent of the scale of the turbulent forcing, within a small range of R_M . We also find that the kinetic alpha, α_K , is subdominant to magnetic alpha, α_M , in the DNS, justifying an assumption in the two scale model. For case (2), we show more comprehensively than in Paper I, how the two scale theory predicts that large scale helical energy at the transition is $E_{c2} = (k_1/k_f)^2 M_{eq}$, where k_1 and k_f are the large scale and small turbulent forcing scale respectively and M_{eq} is the equipartition magnetic energy. The DNS in this case agree qualitatively with the two scale model but the R_M currently achievable, is too small to satisfy a condition $3/R_M \ll (k_1/k_f)^2$, necessary to robustly reveal the transition, E_{c2} . The fact that two scale theory and DNS agree wherever they can be compared and also the two scale theory predicts the transition of case (1) gives us some confidence that E_{c2} of Paper I should be identifiable at higher R_M in DNS as well.

Key words: dynamo–(magnetohydrodynamics) MHD–turbulence–galaxies:magnetic fields–stars:magnet

1 INTRODUCTION

Astrophysical systems, such as stars, galaxies and even galaxy clusters, are observed to host coherent large scale magnetic fields (Clarke et al. 2001; Clarke 2004; Govoni & Feretti 2004; Brandenburg & Subramanian 2005; Vogt & Enßlin 2005; Fletcher 2010; Beck 2012). The origin of such cosmic magnetic fields has been a long standing open question. A popular paradigm is that coherent large scale

magnetic fields arise due to dynamo amplification of small seed fields. An interesting alternative would be if the field from a previous evolutionary phase has simply been flux frozen when a star, galaxy or a galaxy cluster was formed. Astrophysical systems are generally turbulent and such initial fields could then in principle decay due to turbulent diffusion. Indeed due to the above reason, the continued existence of primordial large scale fields in galaxies has been mostly considered to be untenable (Ruzmaikin et al. 1988). However, if coherent magnetic fields in these astrophysical systems were initially of helical nature, and sufficiently strong, Blackman & Subramanian (2013) (henceforth Paper I) argued on the basis of magnetic helicity conservation, that

* palvi@iucaa.ernet.in

† blackman@pas.rochester.edu

‡ kandu@iucaa.ernet.in

they would be resilient to turbulent diffusion and hence, survive up to the present epoch.

If sub-equipartition helical fields can avoid turbulent decay, then another practical implication is that if helical fields are observed in a system—such as astrophysical jets—the observed helical fields would not necessarily be indicative of magnetic energy domination in the system.

Magnetic helicity is a nearly conserved quantity in general astrophysical context and has been useful in understanding of dynamo saturation, by leading to the development of the dynamical quenching formalism (Kleeorin et al. (2000); Field & Blackman (2002); Blackman & Brandenburg (2002); Blackman & Field (2002); Subramanian (2002); Brandenburg & Subramanian (2005) and references therein). Paper I used the large and small scale magnetic helicity evolution equations in a two scale model, along with the mean field induction equation and the minimal τ -approximation, to understand the decay of helical large scale fields. An intriguing result of their work is that even fields which are initially of fairly sub-equipartition strength, would undergo a slow resistive decay if they are helical. It is important to check the validity of this simple two scale model and the results of Paper I, by comparing with results from direct numerical simulations (DNS) of decaying large scale helical magnetic fields in presence of non-helical turbulence. This is the main motivation of the current work.

There have been previous DNS studies of decaying helical fields by Yousef et al. (2003) motivated by trying to understand the quenching of turbulent diffusion. Also, Kemel et al. (2011) discuss simulations of decaying helical fields in non-helical turbulence, applied to the cylindrical geometry. These simulations emphasize the decay of initially strong fields of order equipartition value. On the other hand, Paper I focused on the situation where the initial field strength is lowered to smaller and smaller values and a threshold energy, $E_{c2} = (k_1/k_f)^2 M_{eq}$ was shown to set the transition from slow to fast decay. Here k_1 and k_f are the wave numbers associated with the large scale field and the small turbulent forcing scale, respectively and M_{eq} is the equipartition energy. Such a threshold was not evident in earlier work. We wish to examine here through DNS, the decay of helical field in more generality and with different sets of initial strength and k_f . One motivation is also to examine if there is indeed a k_f dependent threshold energy.

We limit our present study to initially fully helical fields, where the measure of helicity is defined as the ratio of the helical magnetic energy to the the total magnetic energy. As will be evident, there is enough richness and subtlety to be understood here, even without considering fractionally helical cases.

In the next section, we discuss the setup for the simulations and the quantities to be estimated. We find that the large scale helical magnetic field decays in two stages. The first phase is of a slow decay, due to only microscopic resistivity. We discuss the slow regime in detail in Section 2.1. The second phase comprises of fast decay of the large scale magnetic field and is discussed in Section 2.2. We also estimate the transition point which marks the transition from slow to fast decay in section 3. There are two kinds of transition points, arising in two different contexts. One is identified in simulations of decaying field which start with the

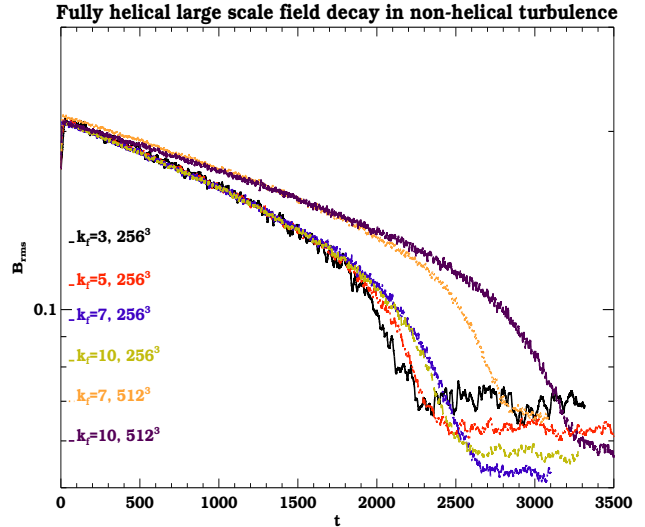


Figure 1. The evolution of B_{rms} in helical magnetic field decay simulations starting with a fully helical field of strength 0.2 (superequipartition). Here, we show the evolution curves for $k_f = 3, 5, 7, 10$ from runs of resolution 256^3 and also from two runs with higher resolution of 512^3 at $k_f = 7$ and 10

same initial field strength (of equipartition value) and resistivity, but different k_f (forcing or the turbulent scale). These show a transition of the evolving field from a slow to fast decay regime after decaying to a critical energy threshold. The other kind could arise in simulations of decaying field, where the initial field strength is decreased until a critical value is reached, below which the field decays at the fast rate right from the beginning. The second kind has been emphasized in Paper I and is discussed in Section 3.2. In general, throughout the paper, we have juxtaposed the results from the simulations with the numerical solutions of the corresponding two scale model from Paper I. A discussion of our results and the conclusions are given in Section 4.

2 SIMULATIONS OF HELICAL LARGE SCALE FIELD DECAY

One of the primary aims of our work is to determine how fast a helical large scale field decays when subject to turbulent diffusion by small scale forcing. We use the PENCIL CODE¹ to simulate the decay of helical large scale fields in the presence of non-helical turbulence. The fluid is assumed to be isothermal, viscous, electrically conducting and compressible. We solve the continuity, Navier-Stokes and induction equations given by,

$$\frac{D \ln \rho}{Dt} = -\nabla \cdot \mathbf{u}, \quad (1)$$

$$\frac{D \mathbf{u}}{Dt} = -c_s^2 \nabla \ln \rho + \frac{\mathbf{J} \times \mathbf{B}}{\rho} + F_{visc} + f, \quad (2)$$

$$\frac{\partial \mathbf{A}}{\partial t} = \mathbf{u} \times \mathbf{B} + \eta \nabla^2 \mathbf{A}. \quad (3)$$

¹ <http://pencil-code.googlecode.com> (Brandenburg 2003)

Here ρ is the density related to the pressure by $P = \rho c_s^2$, where c_s is speed of sound. The operator $D/Dt = \partial/\partial t + \mathbf{u} \cdot \nabla$ is the lagrangian derivative, where \mathbf{u} is fluid velocity field. The induction equation is being expressed in terms of the vector potential, \mathbf{A} and $\mathbf{B} = \nabla \times \mathbf{A}$, is the magnetic field $\mathbf{J} = \nabla \times \mathbf{B}/\mu_0$ is the current density and μ_0 is the vacuum permeability ($\mu_0 = 1$ in the DNS). The viscous force is given by,

$$F_{visc} = \nu \left[\nabla^2 \mathbf{u} + \frac{1}{3} \nabla \cdot \nabla \mathbf{u} + 2S \cdot \nabla \ln \rho \right] \quad (4)$$

where,

$$S = \frac{1}{2} \left(\frac{\partial u_i}{\partial x_j} + \frac{\partial u_j}{\partial x_i} - \frac{2}{3} \delta_{ij} \nabla \cdot \mathbf{u} \right), \quad (5)$$

is the traceless rate of strain tensor. The term $f = f(\mathbf{x}, t)$ is responsible for turbulent forcing localised in k-space in magnitude and randomly changing phase at every time step (see Haugen et al. (2004) for more details). These equations are solved in a Cartesian box of a size $l = 2\pi$ on a cubic grid with N^3 mesh points, adopting periodic boundary conditions.

The initial magnetic field is a Beltrami field, $\mathbf{B} = B(\sin kz, \cos kz, 0)$, where the k is set to 1, in order to place the field at the largest scale in the box. Here k corresponding to the box scale is defined as $k = (2\pi)/l$. In each run, the helical magnetic field is allowed to decay under the influence of a non-helical turbulent forcing. We generate the turbulent flow in the box by randomly forcing the fluid about an average wavenumber k_f , which is much larger than the wavenumber at which the large scale magnetic field is placed. The initial velocity field is zero in all the simulations. We have run a suite of simulations with varying k_f (from 3 to 10), and initial field strength. Most of the simulations have a ‘resolution’ of 256^3 , with 2 higher resolution, 512^3 , runs. The magnetic and fluid Reynolds numbers throughout this paper are defined as $R_M = u_{rms}/\eta k_f$ and $Re = u_{rms}/\nu k_f$, respectively, where η and ν are the resistivity and viscosity of the fluid and are taken to be equal here and hence, $P_M = 1$. Table 1 gives a list of all the simulations run towards the study.

Starting with a helical magnetic field, the rms magnetic field B_{rms} , decays exponentially as shown in Fig. 1, in basically two stages. The field decays at a slow rate first and then transitions to a much faster rate before finally reaching saturation due to the floor provided by the fluctuation dynamo (given that all the simulations have an R_M which is supercritical enabling the fluctuation dynamo to operate (Kazantsev 1967; Haugen et al. 2004; Schekochihin et al. 2004; Bhat & Subramanian 2013)). In the top panel of Fig. 2, we show the evolution of u_{rms} for run B with $k_f = 5$ (considering this to be the fiducial case). The kinetic energy decays by less than 10% along with magnetic field in the first stage. After transition, the magnetic energy decays at a fast rate and as a result, the effect of Lorentz forces on the velocity field is reduced, thus increasing the u_{rms} . In the bottom panel of Fig. 2, the corresponding kinetic energy spectral evolution has been shown at times, $t=10, 100, 2200$ and 2800 , with decreasing line thickness. The peak at $k = 5$ corresponds to the constant forcing.

The corresponding evolution of the magnetic energy spectrum, $M(k)$ for run B with $k_f = 5$, is shown in the top panel of Fig. 3. The top spectrum is at $t=100$ and evolves to

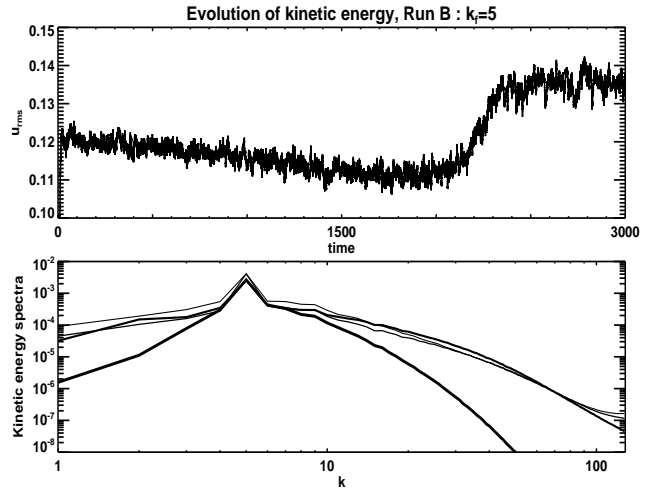


Figure 2. The top panel shows the evolution of u_{rms} with time. It grows to an average initial value of 0.12. In the bottom panel, we show the spectra of the kinetic energy at times $t=10, 100, 2200$ and 2800 for curves with decreasing line thickness respectively.

the bottom at $t=2700$, with an interval of $\Delta t=200$ between successive spectra. Initially, the total helicity and the associated helical energy is on $k = 1$, which is then transferred to smaller scales, on time scale of few eddy turn over times. In the bottom panel of Fig. 3, we show the fractional helicity spectrum, defined as the ratio of helical energy, $kH(k)/2$ to magnetic energy, $M(k)$, where $H(k)$ and $M(k)$ are the magnetic helicity and energy spectra respectively. We find that the helicity on the small scales is of the same sign as that on the large scale, as can be seen in the bottom panel of Fig. 3. The upper three curves corresponding to times, $t=100, 1100, 2100$ show that in the large scales, the energy is almost fully helical. And the fractional helicity in small scales is < 1 , due to the non-helical energy being constantly pumped at $k = k_f$ (where $k_f > k_1$), due to the non helical forcing. By $t=2700$, corresponding to the bottom most spectrum of highest thickness, the large scale field has almost decayed completely. And hence, the sign of helicity is fluctuating across all scales.

The constant non-helical forcing at k_f , generates turbulence and subsequently facilitates the transfer of helicity and energy from k_1 to smaller scales. And then it becomes imperative to identify the ‘large’ scale field, to be able to analyse the simulation results. We consider contributions from $k = 1$ to $k = 2$, to form the large scale field. This seems an appropriate choice given that the power spectra of various quantities like magnetic energy and magnetic helicity, have a minimum at $k=2$ and peak again at $k = k_f$ as can be seen from Fig. 3. Consequently, for $k > 2$, the spectral energy has been considered to be a part of the small scale field.² Thus each variable is split into a large scale (mean) and small scale (fluctuating) quantity, with an overbar de-

² It is difficult to decide an unambiguous scale separation between the large and small in general. But in cases such as the α^2 dynamo, the scale separation can be decided based on the opposite sign of helicity on the two scales (Brandenburg & Subramanian

Table 1. All the simulations have $u_{rms} = 0.12$ and start with the fully helical magnetic field of strength $B_{rms} = 0.2$. The runs are at $P_M = 1$. Also $\bar{\gamma}$ is the average initial decay rate.

Run	Resolution	k_f	$\eta \times 10^4$	R_M	M_0	$\bar{\gamma}$
A	256^3	3	2.0	200	1	0.0009
B	256^3	5	2.0	120	1	0.0009
C	256^3	7	2.0	86	1	0.0009
D	256^3	10	2.0	60	1	0.0009
E	512^3	7	1.5	120	1	0.0007
F	512^3	10	1.5	80	1	0.0007
G	256^3	5	2.0	120	1/5	0.003
H	256^3	5	2.0	120	1/10	0.004
I	256^3	5	2.0	120	1/20	0.008
J	256^3	5	2.0	120	1/25	0.010
K	256^3	5	2.0	120	1/50	0.016

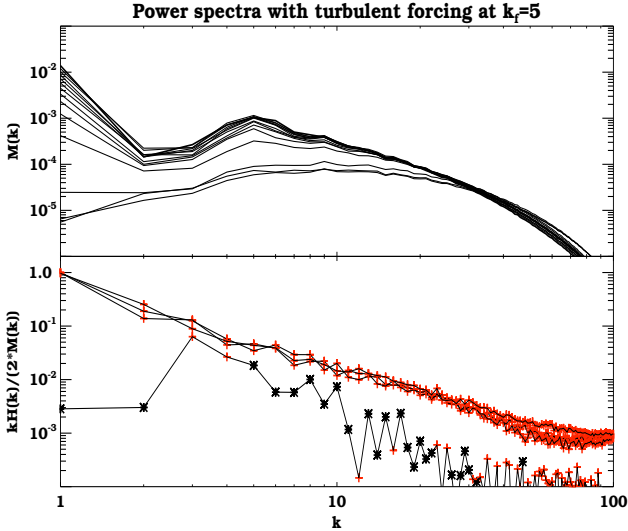


Figure 3. The top panel shows the evolving magnetic power spectra, $M(k)$ for run B. Spectral evolution has been plotted from top to bottom, corresponding to times, $t=100$ to $t=2700$, with an interval of $\Delta t = 200$, between subsequent spectra. The bottom panel shows the ratio of helical energy, $kH(k)/2$ to the magnetic energy, $M(k)$. The red 'plus' symbol indicates a positive value, and the black star indicates a negative value. The four curves from top to bottom are at times $t=100, 1100, 2100$ and 2700

noting the mean; for example the magnetic field $\mathbf{B} = \bar{\mathbf{B}} + \mathbf{b}$, where $\bar{\mathbf{B}}$ and \mathbf{b} are respectively the large and small scale fields. Further, we will consider volume averages of several quadratic quantities like magnetic energy density over the whole simulation box, and denote such averages by angular brackets $\langle \rangle$.

The three quantities we are mainly interested in are the following. First, the total large scale magnetic energy, $\langle \bar{\mathbf{B}}^2 \rangle / 2$, defined as,

$$\frac{\langle \bar{\mathbf{B}}^2 \rangle}{2} = \int_1^2 M(k) dk. \quad (6)$$

2005; Brandenburg 2011). In our case as shown in Fig. 3, the helicity on both the scales are of the same sign.

Second, large scale helical energy (LSHE), M_H ,

$$M_H = \int_1^2 \frac{kH(k)}{2} dk. \quad (7)$$

This is an important quantity because the two scale model from Paper I is applied to study the evolution of LSHE. And then the behaviour of LSHE can be extended to the total large scale energy, $\langle \bar{\mathbf{B}}^2 \rangle / 2$, upto some time scale. Third, small scale helicity (SSH), $\langle \mathbf{a} \cdot \mathbf{b} \rangle$,

$$\langle \mathbf{a} \cdot \mathbf{b} \rangle = \int_2^\infty H(k) dk \quad (8)$$

An important understanding derived from the two scale model is that the SSH remains in steady state for most of the slow decay phase. And the transition from slow to fast decay is largely governed by the change in SSH. And hence it is critical to check the nature of SSH evolution in the DNS.

We show the time evolution of $\langle \bar{\mathbf{B}}^2 \rangle / 2$, M_H and $\langle \mathbf{a} \cdot \mathbf{b} \rangle$ in Fig. 4 for runs A, B, C and D with a resolution of 256^3 . All these quantities have been normalised by the equipartition energy $M_{eq} = \rho u_{rms}^2 / 2$, with $\rho \approx 1$ in the simulation units.

These runs have the same η , but different k_f and hence different R_M (see Table 1). In Fig. 5, we show the time evolution of these three quantities in higher resolution (512^3) runs E and F. In the upper panels of Fig. 4 and Fig. 5, the evolution of the total large scale energy, $\langle \bar{\mathbf{B}}^2 \rangle / 2$, is shown in dot-dashed red line and the LSHE, M_H , is shown in solid black, along with the solution for M_H from the two scale model in blue dashed line. (The evolution equations for the two scale model are given below). In the lower panels, the dotted red line shows evolution of SSH, $\langle \mathbf{a} \cdot \mathbf{b} \rangle$. One can observe that the gap between the curve for the two quantities, $\langle \bar{\mathbf{B}}^2 \rangle / 2$ and M_H increases once the helicity has decreased substantially in the fast decay phase. Also, the gap becomes more pronounced for smaller k_f runs due to the smaller scale separation.

The decay rate in a particular decay phase is calculated by two methods. One is by simply fitting an exponential form to the $M_H(t)$, given by,

$$M_H(t) = M_{H0} e^{-\gamma t} \quad (9)$$

where M_{H0} and γ are the free parameters. Note that we retain the code time scale, t , while plotting the decay curves in the Fig. 4 and Fig. 5. Here, $t = k_1 c_s$, where $k_1 = 1$.

It can be seen from Fig. 4 and Fig. 5, that slope of LSHE evolution curve is changing continuously. Thus, the decay rate obtained by the first method, will be an average estimate. In the second method, we fit for the entire LSHE evolution curve, using the function,

$$M_H(t) = \exp\left(\frac{1}{A+Bt} + \frac{1}{C+Dt}\right) \quad (10)$$

where A, B, C and D are free parameters.³ Then the logarithmic slope of LSHE is derived from the fit. This gives the decay rate as a function of time.

In both methods of estimating the decay rate, best fits were decided by the calculation of least squares. We now discuss the two phases of decay.

³ Other fitting forms were tried, to fit the entire curve of LSHE evolution. This form provides the best fit by the method of least squares.

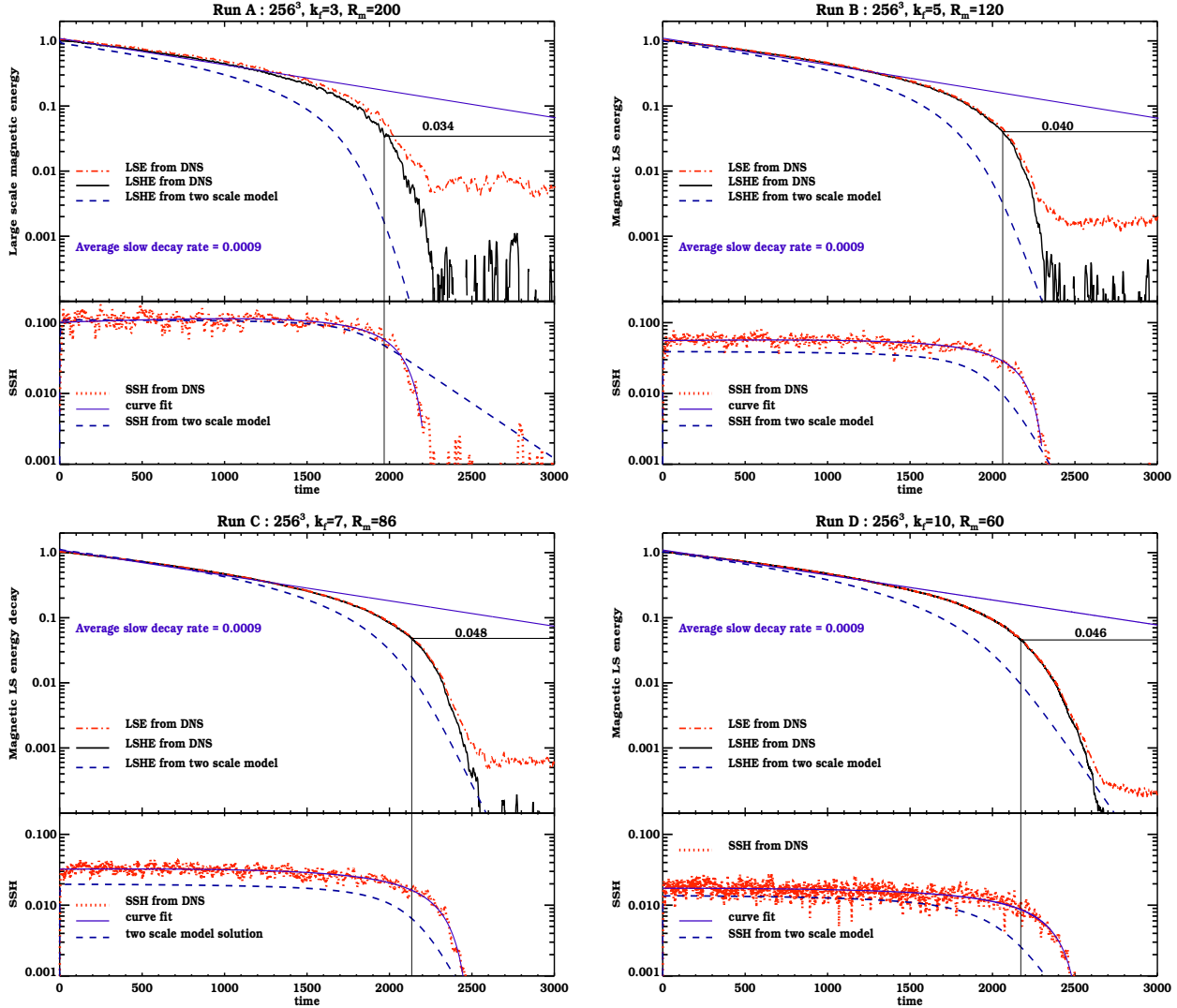


Figure 4. We show the evolution of $\langle \overline{\mathbf{B}^2} \rangle / 2$, M_H and $\langle \overline{\mathbf{a} \cdot \mathbf{b}} \rangle$ for runs with 256^3 resolution at $k_f = 3, 5, 7$ and 10 . All the quantities are normalised by M_{eq} . The thin vertical line marks the time by when the SSH decreases by 50% of its initial steady state value, in the bottom panel and intersects the LSHE curve at the transition energy indicated by the horizontal thin line. The thin blue line shows the fit using Eq. 9 to the slow decay phase.

2.1 Slow decay phase

The purely resistive decay rate for the large scale magnetic energy $k_1 = 1$ mode is given by $2\eta k_1^2 = 4 \times 10^{-4}$ (in dimensionless units) for runs A to D with $\eta = 2 \times 10^{-4}$. The slow decay regime for assessing the average decay rate is identified from $t = 0$ to $t = t_{slow}$, where $t = t_{slow}$ is chosen as an arbitrary time comfortably less than the time, the curve evolves towards the transition region.

From the exponential fit to the initial slow decay regime, the average decay rate, $\gamma_S \sim 9 \times 10^{-4}$, is almost twice the purely resistive decay rate for $k_1 = 1$ (where the large scale field resides). Nevertheless, this γ_S is much smaller than the corresponding turbulent decay rate $\sim 2\eta_t k_1^2 = (2/3)u_{rms}/k_f$. For example, in the fiducial case of run B, where $k_f = 5$ and with $u_{rms} = 0.12$, we have $(2/3)u_{rms}/k_f = 0.016$, which is ~ 18 times larger than the γ_S obtained from DNS. Notice that the initial field is quite close to the equipartition strength. This goes to show that

helical magnetic field of a sufficiently large initial strength, decays slowly at a rate which is of the order of the resistive time-scale and does not decay turbulently as one may have naively expected.

In the top panel of Fig. 6, we show the fit to LSHE evolution curve for runs A-D, using the form in Eq. 10. In the bottom panel of Fig. 6, we show the logarithmic slope of LSHE from the fit. On taking the mean of the logarithmic slope values in the resistive decay phase (from $t = 0$ to $t = t_{slow}$), we again obtain the average estimate of $\gamma_S \sim 9 \times 10^{-4}$. Hence matching with the γ_S obtained from the first method. Nonetheless, as can be seen from Fig. 6, the decay rate is continuously changing even in the slow decay phase. This slowly changing decay rate can be understood by considering the following.

The large scale field in the simulations is almost fully helical. Hence the large scale field is expected to decay according to the equations governing the evolution of magnetic

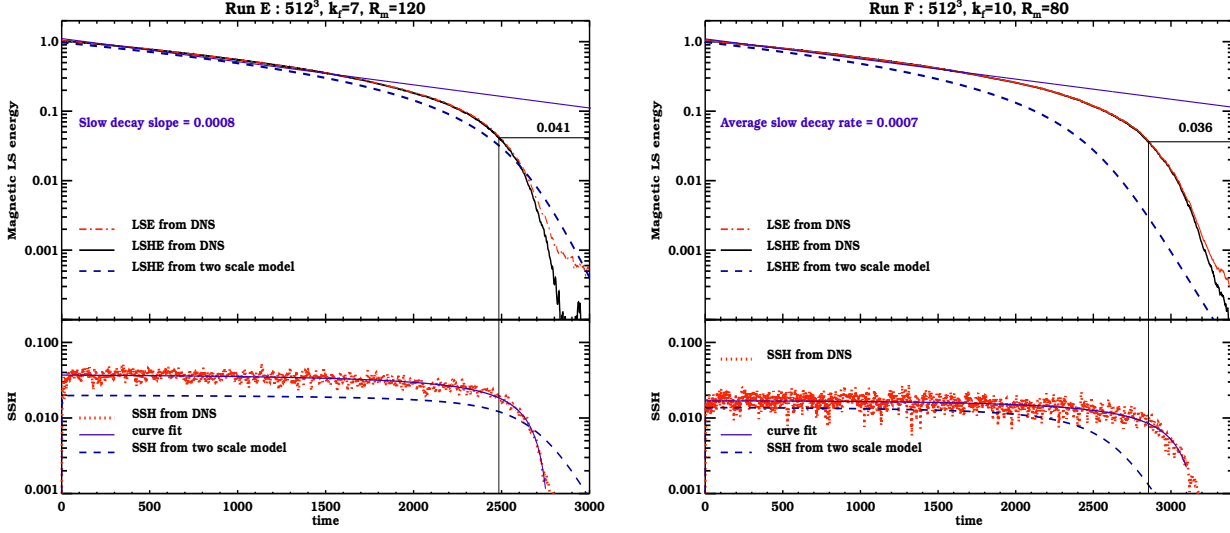


Figure 5. We show the evolution of $\langle \overline{\mathbf{B}^2} \rangle / 2$, M_H and $\langle \overline{\mathbf{a} \cdot \mathbf{b}} \rangle$ for runs with 512^3 resolution at $k_f = 7$ and 10 . All the quantities are normalised by M_{eq} . The thin vertical line marks the time by when the SSH decreases by 50% of its initial steady state value, and intersects the LSHE curve at the transition energy indicated by the horizontal thin line. The thin blue line shows the fit using Eq. 9 to the slow decay phase.

helicity (which is a conserved quantity in the limit of $\eta \rightarrow 0$). For periodic or closed domains, evolution of the total magnetic helicity is given by,

$$\frac{d\langle \overline{\mathbf{A} \cdot \mathbf{B}} \rangle}{dt} = -2\eta \langle \overline{\mathbf{J} \cdot \mathbf{B}} \rangle \quad (11)$$

All the quantities can be split into a mean (large scale) and a fluctuating (small scale) component. Accordingly, Eq. 11 can be written as,

$$\frac{d\langle \overline{\mathbf{A} \cdot \mathbf{B}} \rangle}{dt} + \frac{d\langle \overline{\mathbf{a} \cdot \mathbf{b}} \rangle}{dt} = -2\eta (\langle \overline{\mathbf{J} \cdot \mathbf{B}} \rangle + \langle \overline{\mathbf{j} \cdot \mathbf{b}} \rangle) \quad (12)$$

where cross terms between the large and small scales vanish. Now, the small scale magnetic helicity is expected to reach steady state much faster than the large scale magnetic helicity. And hence, if $d\langle \overline{\mathbf{a} \cdot \mathbf{b}} \rangle / dt \rightarrow 0$ (as can be seen from Fig. 4), then large scale magnetic helicity decays at a rate decided by both $\langle \overline{\mathbf{J} \cdot \mathbf{B}} \rangle$ and $\langle \overline{\mathbf{j} \cdot \mathbf{b}} \rangle$.

To obtain an equation for large scale helicity, one can use the mean field induction equation, given as,

$$\frac{\partial \overline{\mathbf{B}}}{\partial t} = -c \nabla \times \overline{\mathbf{E}} = \nabla \times (\overline{\mathbf{v}} \times \overline{\mathbf{B}} + \mathcal{E} - \eta \nabla \times \overline{\mathbf{B}}) \quad (13)$$

where, $\mathcal{E} = \overline{\mathbf{v} \times \mathbf{b}}$ is the electromotive force (or the EMF). Using the first order smoothing approximation (FOSA) (Moffatt 1978; Krause & Raedler 1980) or a τ -approximation closure scheme (Pouquet et al. 1976; Blackman & Field 2002; Rädler et al. 2003; Brandenburg & Subramanian 2005), \mathcal{E} can be shown to be given by,

$$\mathcal{E} = (\alpha_K + \alpha_M) \overline{\mathbf{B}} - \eta_t \overline{\mathbf{J}}. \quad (14)$$

Here the kinetic alpha effect (α_K), magnetic alpha effect (α_M) and the turbulent diffusivity (η_t) are given by,

$$\alpha_K \simeq -\frac{\tau}{3} \overline{\mathbf{v} \cdot \boldsymbol{\omega}}, \quad \alpha_M \simeq \frac{\tau}{3\rho} \overline{\mathbf{j} \cdot \mathbf{b}}, \quad \eta_t \simeq \frac{\tau}{3} \overline{\mathbf{v}^2} \quad (15)$$

and τ is the correlation time which can be estimated to

be of order the dynamical or eddy turn over time, $t_{eddy} = 1/(u_{rms} k_f)$. We uncurl Eq. 13 to obtain an equation for the mean vector potential, $\overline{\mathbf{A}}$. This can be used to obtain the dynamical equation for large scale helicity,

$$\frac{1}{2} \frac{d\langle \overline{\mathbf{A} \cdot \mathbf{B}} \rangle}{dt} = \langle (\alpha_K + \alpha_M) \cdot \overline{\mathbf{B}^2} \rangle - \eta_t \langle \overline{\mathbf{J} \cdot \mathbf{B}} \rangle - \eta \langle \overline{\mathbf{J} \cdot \mathbf{B}} \rangle \quad (16)$$

where we have put divergence terms to zero for periodic boundary conditions. The SSH evolution is obtained by subtracting Eq. 16 from Eq. 12,

$$\frac{1}{2} \frac{d\langle \overline{\mathbf{a} \cdot \mathbf{b}} \rangle}{dt} = -\langle (\alpha_K + \alpha_M) \cdot \overline{\mathbf{B}^2} \rangle + \eta_t \langle \overline{\mathbf{J} \cdot \mathbf{B}} \rangle - \eta \langle \overline{\mathbf{j} \cdot \mathbf{b}} \rangle \quad (17)$$

From Eq. 16, we see that the large scale helical field would decay due to turbulent diffusion in the absence of the alpha effect. In our context of forced non-helical turbulence, the kinetic alpha effect is expected to be negligible. We verify this below, directly from DNS, in section 2.3. However, α_M could be generated by the action of turbulent diffusion on a large scale helical field. This can be seen explicitly in the term, $\eta_t \langle \overline{\mathbf{J} \cdot \mathbf{B}} \rangle$ in Eq. 17, which leads to the generation of $\langle \overline{\mathbf{a} \cdot \mathbf{b}} \rangle$ and hence $\langle \overline{\mathbf{j} \cdot \mathbf{b}} \rangle$ (even if were initially zero), having the same sign as $\langle \overline{\mathbf{J} \cdot \mathbf{B}} \rangle$. Thus, the resulting α_M can in principle, balance the turbulent diffusion leading to a slow resistive decay of the LSHE. This implicitly constitutes large scale dynamo action, driven by the small scale current helicity.

We also see from Eq. 17, that $-\langle \alpha_M \cdot \overline{\mathbf{B}^2} \rangle \propto -k_f^2 \langle \overline{\mathbf{a} \cdot \mathbf{b}} \rangle \langle \overline{\mathbf{B}^2} \rangle$, causes rapid damping of the SSH and leads to a steady state. For such a steady small scale helicity, Eq. 17 can be used to derive a relation between, $\langle \overline{\mathbf{J} \cdot \mathbf{B}} \rangle$ and $\langle \overline{\mathbf{j} \cdot \mathbf{b}} \rangle$. We have for $d\langle \overline{\mathbf{a} \cdot \mathbf{b}} \rangle / dt \rightarrow 0$,

$$0 = -\alpha_M \langle \overline{\mathbf{B}^2} \rangle + \eta_t \langle \overline{\mathbf{J} \cdot \mathbf{B}} \rangle - \eta \langle \overline{\mathbf{j} \cdot \mathbf{b}} \rangle \quad (18)$$

where, we have dropped the kinetic alpha term following Paper I. And by substituting the expression for α_M into

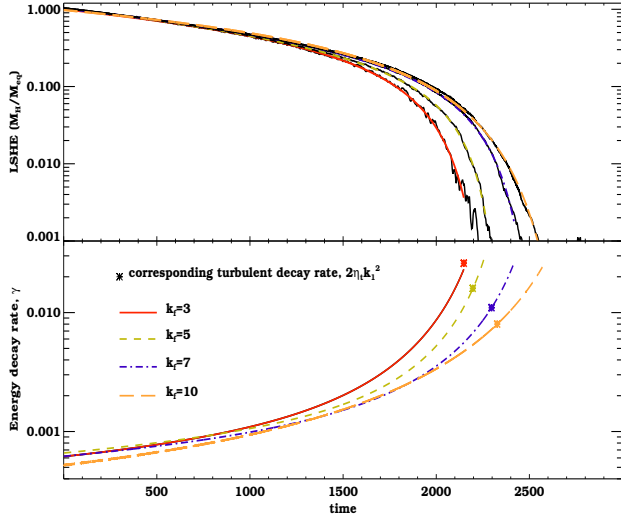


Figure 6. Top panel shows the normalised LSHE evolution for runs A-D along with the fit using the function in Eq. 10. Bottom panel gives the logarithmic derivative using the fit, i.e. the decay rate evolution for all runs. The symbol, *, in the bottom panel, marks the value of respective turbulent decay rates.

Eq. 18, we have,

$$\langle \mathbf{j} \cdot \mathbf{b} \rangle = \frac{\langle \mathbf{J} \cdot \mathbf{B} \rangle}{\frac{\eta}{\eta_t} + \frac{\langle \mathbf{B}^2 \rangle / 2}{M_{eq}}} \quad (19)$$

where, M_{eq} is equal to $\rho u_{rms}^2 / 2$, in dimensionless units.

In the denominator of the RHS of the Eq. 19, if one considers that $\eta \ll \eta_t$, and hence negligible, then with $\langle \mathbf{B}^2 \rangle / 2 M_{eq} = 1$ (which is the case initially in the runs A-F), we have $\langle \mathbf{j} \cdot \mathbf{b} \rangle \simeq \langle \mathbf{J} \cdot \mathbf{B} \rangle$. This implies that from Eq. 12, with $d\langle \mathbf{a} \cdot \mathbf{b} \rangle / dt \rightarrow 0$, the LSHE decays at twice the resistive decay rate. This is an average estimate as $\langle \mathbf{B}^2 \rangle / 2$ is actually decaying slowly, and hence, $\langle \mathbf{j} \cdot \mathbf{b} \rangle / \langle \mathbf{J} \cdot \mathbf{B} \rangle$ will increase over time, increasing the decay rate as can be seen from the bottom panel of Fig. 6. So, in fact the decay rate of LSHE is changing continuously even in the slow decay phase.

To further corroborate this continuous change in decay rate from theory, consider the following: Using the Eq. 19, we show in Fig. 7, an estimate of the quantity $M = \langle \mathbf{B}^2 \rangle / 2 M_{eq} = \langle \mathbf{j} \cdot \mathbf{b} \rangle / \langle \mathbf{J} \cdot \mathbf{B} \rangle - \eta / \eta_t$, for run B as a solid yellow line. While LSHE calculated directly using Eq. 7 is shown in solid black. Then, we use the function in Eq. 10 to fit for both LSHE and M . Subsequently, we derive the logarithmic slope of the evolution curves using the fit and have shown them as black and yellow dash-dotted lines for direct LSHE and M , respectively. While the amplitude of the curve for M is smaller than that of direct LSHE by $\sim 30\%$, the decay rate evolution predicted by M , matches closely with that of direct LSHE for most of the resistive decay phase. And we can see directly from Fig. 7, that decay rate is increasing constantly by a small amount for most of the slow decay phase. The match in the decay rate evolution of M_H with that from the model M , shows that the two scale model is quite useful for understanding the simulation results in the slow decay phase.

Note that the Fig. 7 of Kemel et al. (2011), shows

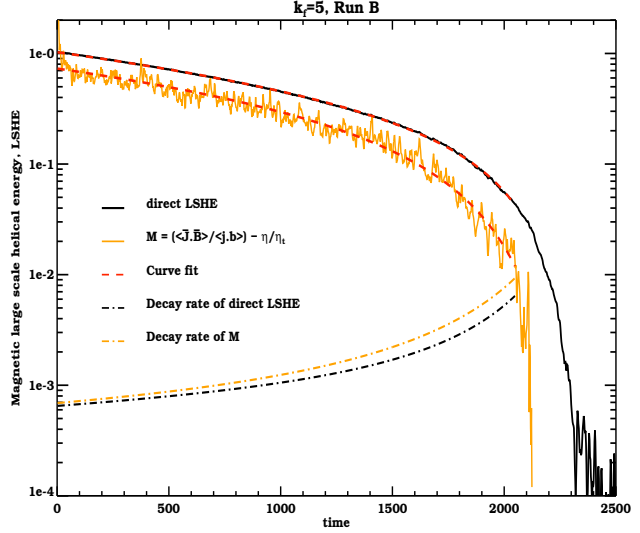


Figure 7. The normalised LSHE evolution curve is overlaid by the predicted noisier LSHE from the two scale model, as according to the Eq. 19, in the fiducial case of run B. The dashed curves are the corresponding logarithmic slopes evaluated using the fit for each of the LSHE curves.

the decay of a highly superequipartition field with time. They find the initial decay rate for the magnetic energy to be $\gamma = -2\eta k_1^2$ (while we obtain the decay rate of $4\eta k_1^2$ for equipartition initial fields). For $\langle \mathbf{B}^2 \rangle / 2 \gg M_{eq}$, from Eq. 19, $\langle \mathbf{j} \cdot \mathbf{b} \rangle \ll \langle \mathbf{J} \cdot \mathbf{B} \rangle$ and hence the large scale field is then predicted to decay at a purely resistive rate, which is consistent with their finding.

In passing we also note that the correct prediction of the rate of slow decay, γ_S by the two scale model, which uses the closure relation for \mathcal{E} in the Eq. 16, also lends some credence to such mean field closures.

2.2 Fast decay phase

We see from Fig. 4 that the LSHE decays at a much faster rate after it drops below some critical energy threshold. The fast decay phase is identified from some time after the curved transition region, to the time just before the field saturates, to a level determined by the tail of the fluctuation dynamo at large scales. (A more precise definition of the transition to the fast decay regime follows in section 3). Here the expected decay rate is the turbulent decay rate, $\gamma_F = 2\eta_t k_1^2$, where $\eta_t = u_{rms} / 3k_f$. In the simulations, $u_{rms} = 0.12$ and $\eta_t = 0.027$ for run A, $\eta_t = 0.016$ for run B, $\eta_t = 0.011$ for run C and $\eta_t = 0.008$ for run D. The two scale model solutions match with expected decay rate of $2\eta_t k_1^2$ and are shown as the blue dashed lines in Fig. 4. It can be seen from Fig. 4, that in almost every DNS run, the slope of the LSHE curve in fast decay phase, is steeper than that of the two scale model solution. In fact, we find that the decay rate in the fast decay phase does not settle to a specific value, but keeps increasing with time, until the LS energy has decreased sufficiently to be dominated by noise.

The top panel of Fig. 6 shows that the fit for LSHE evolution curve does not reach an asymptotic slope at late times. The logarithmic slope of the large scale energy derived

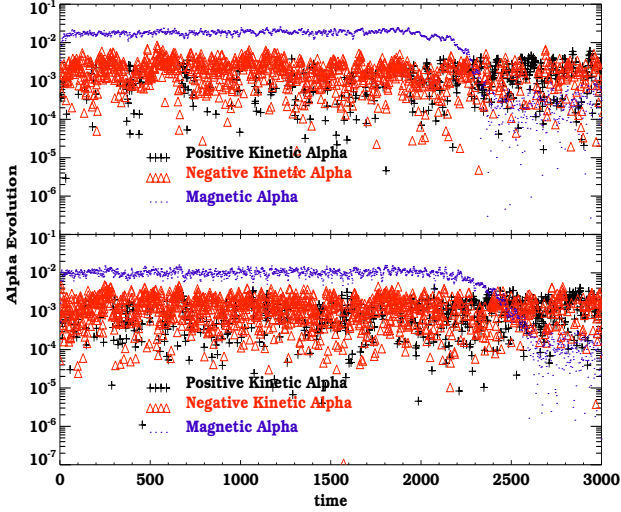


Figure 8. The top and bottom panels show α_K and α_M against time in the simulations, with $k_f=5$ and $k_f=10$ respectively.

from the fit is shown in the bottom panel of Fig. 6. It can be seen that for runs B-D, the logarithmic slope goes to values much larger than the turbulent decay rate. In all these cases, the large scale and small scale is constituted by a sharp split at $k = 2$. However, this is an imperfect split and the effective large scale wave number, k_1 could increase to a higher value, as the large scale field decays. Such an increase in the wavenumber for 'large scale' would then increase the expected turbulent rate.

Fig. 4 also shows SSH evolution obtained in the DNS with different k_f . Initially SSH is zero in the DNS, but rises to a non-zero value due to transfer of helicity from large to small scales and then stays roughly constant before decaying at late times. Paper I predicts the initial value for the steady state SSH, to be $(k_1/k_f^2)M_{eq}$. The corresponding two scale solutions are shown as dashed lines in the Fig. 4, and we see that the steady SSH come close to expected values, but are larger in DNS runs B-F. This shows the limitations of the two scale model in capturing the whole spectral evolution of the DNS, nevertheless there is a reasonable agreement with expectations of the two model. Also, we find that the second slope of SSH, after the steady state phase, is steeper than the corresponding two scale model slope. Here again we expect that the effective wavenumber for small scale field increases from k_f to larger values, resulting in a faster decay of SSH in the DNS. Whereas such an increase would be restricted in the two scale model, where the small scale is fixed at k_f .

2.3 Effects of kinetic alpha

Paper I has discussed at length, the contribution of kinetic alpha, α_K to \mathcal{E} . In the derivation leading to the two scale model, it was assumed the contribution of α_K to \mathcal{E} is negligible as compared to α_M . The kinetic alpha, α_K , could be generated due to the Lorentz force and then would oppose the magnetic alpha, α_M . If α_K was significant, then the large scale helical field would decay much faster than the resistive decay rate. It was argued in Paper I that the generated α_K is indeed small. Nonetheless, it is important

to make an estimate of α_K from the DNS and quantify its contribution to the net \mathcal{E} .

In Fig. 8, we show both α_K and α_M estimated from the DNS using Eq. 15. It can be seen that α_K fluctuates but is mostly negative and opposite in sign compared to α_M in the slow decay phase. One also sees from the Fig. 8, that α_K in the slow decay phase is found to be a factor of 4-5 smaller than α_M in the case of $k_f = 5$ (Run B) and a factor of ~ 10 smaller in the case of $k_f = 10$ (Run D). The contribution of α_K to the EMF is thus considerably smaller than α_M and hence subdominant as argued in Paper I. In the saturated phase, when all the magnetic helicity (and hence, α_M) has decayed, the α_K alternates equally between being positive and negative values.

3 THE TRANSITION POINT

It is important to identify the threshold below which the slow decay turns into a fast one, because smaller the transition energy is with respect to equipartition value, longer would be the timescale for which the helical large scale field remains resilient to turbulent diffusion.

We identify two kinds of transition energy, E_{c1} and E_{c2} , arising in two different contexts. One threshold E_{c1} , arises in the context where as the field decays in time, it transits from the slow decay phase to the fast decay phase after crossing the threshold energy, E_{c1} . This behaviour is what has been examined so far, in runs A-F, where we started with a field of equipartition strength. The other context is where one starts with different initial large scale field strengths. As initial magnetic energy is decreased, below a threshold, E_{c2} , the field ceases to start with resistive decay phase and instead decays at a much faster rate right from the beginning. Paper I argued on the basis of two scale model that the latter threshold or critical energy is k_f dependant with $E_{c2} = (k_1/k_f)^2 M_{eq}$. We will examine both types of transition points. We first focus on E_{c1} in section 3.1 and later on E_{c2} in Section 3.2.

3.1 Transition emerging at late times from an initially resistively decaying field

To identify this transition, we first consider the two scale model and then turn to the DNS. We solve numerically Eq. 16 and Eq. 17 of the two scale model, for different k_f , and then plot the time evolution of the large scale magnetic energy. To explore the behaviour of the transition point under the variations in k_f alone, we keep R_M and the initial magnetic energy, M_0 fixed across different numerical solutions. In the left hand side panel of Fig. 9, we show the decay of a fully helical large scale field with time for different $k_f = 3, 5, 7, 10, 20$. The initial magnetic energy, $M_0 = M_{eq}$ and the R_M is fixed to a value of 120 which is comparable to the value in the DNS. One immediately notices that all the curves almost coincide. Note that in these solutions, the η is the same, which explains the same slope in the slow decay regime. And in order to keep the turbulent decay rate, $\sim 2u_{rms}k_1^2/3k_f = 2u_{rms}/3k_f$, the same, we compensate the increasing k_f , by increasing the u_{rms} . This forms the ideal experiment to understand the behaviour of the transition

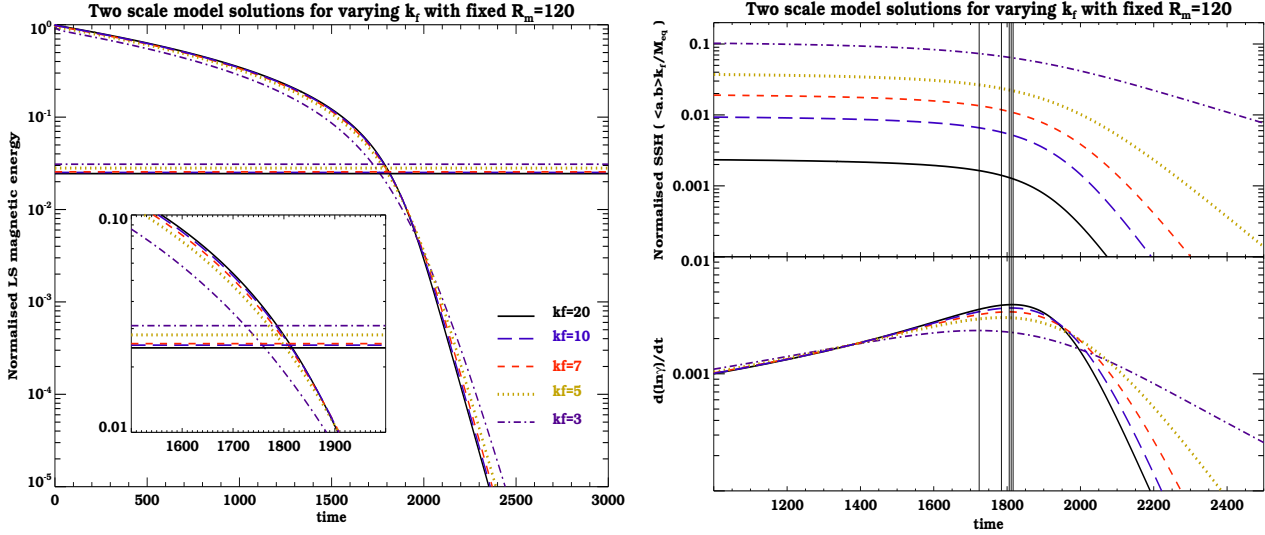


Figure 9. For panel in the left, two scale model solutions for normalised LSHE is given for varying k_f , at 3,5,7,10,20. Panel in the right shows the corresponding two scale model solutions for normalised SSH. R_M is fixed at 120.

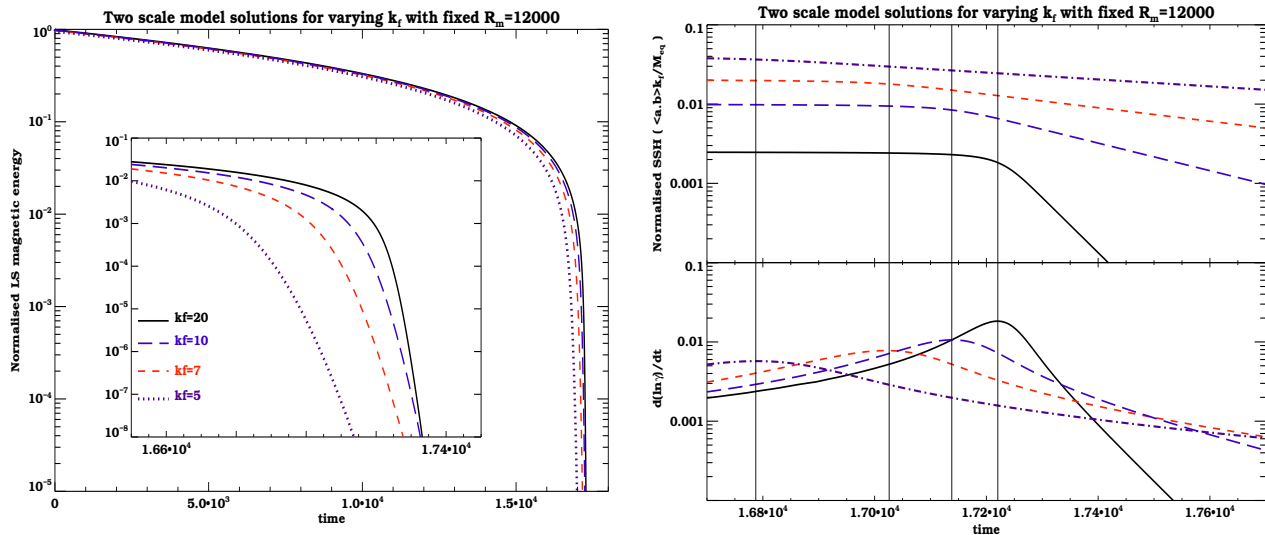


Figure 10. For panel in the left, two scale model solutions for normalised LSHE is given for varying k_f , at 5,7,10,20. Panel in the right shows the corresponding two scale model solutions for normalised SSH. R_M is fixed at 12000.

point as k_f is varied. From the left panel of Fig. 9, the behaviour of the transition point is seen to be independent of the changing turbulent forcing scale, k_f .

To determine the transition point, we have adopted the following method. The evolving decay rate of the large scale helicity, from the two scale model is given by,

$$\gamma = \frac{1}{2\langle \mathbf{A} \cdot \mathbf{B} \rangle} \frac{d\langle \mathbf{A} \cdot \mathbf{B} \rangle}{dt} = -\eta_t k_1^2 \left(1 - \frac{k_f^2 \langle \mathbf{a} \cdot \mathbf{b} \rangle}{k_1 M_{eq}} \right) - \eta k_1^2 \quad (20)$$

where, for fully helical fields, $\langle \mathbf{J} \cdot \mathbf{B} \rangle \sim k_1^2 \langle \mathbf{A} \cdot \mathbf{B} \rangle$ and $\langle \mathbf{j} \cdot \mathbf{b} \rangle \sim k_f^2 \langle \mathbf{a} \cdot \mathbf{b} \rangle$. Also, $\langle \mathbf{B}^2 \rangle \sim k_1 \langle \mathbf{A} \cdot \mathbf{B} \rangle$ and therefore, Eq. 20 also describes the evolving decay rate of the large scale energy. The decay rate is expected to be fairly constant in the slow decay phase and sharply increases during the transition region and then settles to the turbulent de-

cay value. Thus, the logarithmic slope of γ will go through a maximum, when the decay rate changes the fastest. The point in time when the maximum occurs, can be then defined as the point of transition and the corresponding large scale energy is defined to be the transition energy. In the bottom right panel of Fig. 9, we show the $d(\ln \gamma)/dt$ curves, while the top right panel shows the evolution of SSH. Note also that the maximum of $d(\ln \gamma)/dt$ coincides with the point at which the SSH changes slope, i.e. SSH goes from nearly steady state value to decaying resistively at k_f . We thus find the transition energy to be $E_{c1}/M_{eq} = 0.031, 0.029, 0.026, 0.025, 0.025$ for $k_f = 3, 5, 7, 10, 20$ respectively. For completeness, along with the Eq. 20, we give here the corre-

sponding equation for the small scale helical field,

$$\frac{1}{2} \frac{d \ln(\langle \mathbf{a} \cdot \mathbf{b} \rangle)}{dt} = -\eta_t k_f^2 \frac{(k_1 \langle \overline{\mathbf{A}} \cdot \overline{\mathbf{B}} \rangle)}{M_{eq}} \left(1 - \frac{k_1 M_{eq}}{k_f^2 \langle \mathbf{a} \cdot \mathbf{b} \rangle} \right) - \eta k_2^2 \quad (21)$$

In Fig. 10, we show similar plots of two scale solutions at a much larger $R_M = 12000$, to also test the sensitivity of the results with respect to changes in R_M . The right panel of the Fig. 10, shows at the top, evolution of SSH while the bottom panel shows the evolution of $d(\ln\gamma)/dt$. It can be seen from such plots for both the cases of $R_M = 120$ and 12000, that as the k_f increases, the point at which SSH changes slope, occurs later in time. And the corresponding large scale energy curve also transitions later in time. As a result, the transition energy would be similar across different k_f . The transition energy estimated in this case is $E_{c1}/M_{eq} = 0.0011, 0.0009, 0.0009, 0.0008$ for $k_f = 5, 7, 10, 20$ respectively. We find that the change in the transition energy from $R_M = 120$ to $R_M = 12000$ is by a factor of $\sim 25 - 30$. Thus interestingly, E_{c1} seems to scale as $R_M^{-1/2}$.

Now we turn to the DNS and determine the transition energy of type E_{c1} for the various runs in Table 1. In the case of simulations, we find that the decay rate in fast regime, is changing with time and does not settle to a final value as is the case in the two scale model. Therefore, we do not find a maximum in the evolving logarithmic slope of LSHE to be able to determine the transition point. Instead, we adopt a slightly different method of estimating the transition energy in the case of DNS. From the right panels of Fig. 9 and Fig. 10, we pointed out that $d(\ln\gamma)/dt$ is maximum when the SSH begins to decrease. Thus it seems plausible to define the transition point as the time when the SSH decreases from its initial steady state value by say, 50%. From Eq. 20, it can be seen that the first term on RHS goes to 0 when $\langle \mathbf{a} \cdot \mathbf{b} \rangle = (k_1/k_f^2)M_{eq}$ is in steady state, and by the time SSH, $\langle \mathbf{a} \cdot \mathbf{b} \rangle$ decreases by 50%, the large scale field is expected to decay at a rate, of the order of the turbulent decay rate.

We use again the form in Eq. 10 to determine a fit for the SSH evolution. Then we estimate the point in time by when SSH decreases by 50% of its initial steady state value. The corresponding value of large scale energy is the transition energy. This method of determining the transition energy is conceptually similar to the one used for two scale model as it determines the point at which there is a change in the SSH evolution from steady state (or nearly zero decay rate) to a non-zero decay rate. This method of determining the transition energy is illustrated in the lower panels of Fig. 4 and Fig. 5. The vertical lines in these figures give the time when SSH has decreased by 50% of its initial steady state value. This line intersects the LSHE curve at a transition energy value indicated by the horizontal line in each upper panel of Fig. 4 and Fig. 5. The transition energy thus determined, gives the critical energy as $E_{c1} \sim 0.034 M_{eq}$ for run B. This is similar to the transition point we obtain from the corresponding two scale model solution of $E_{c1} \sim 0.029 M_{eq}$. For the other runs A, C, D, E and F we find the transition energy to be $E_{c1}/M_{eq} = 0.052, 0.049, 0.048, 0.037$ and 0.034 respectively, as can be read from the Fig. 4 and Fig. 5. This indicates the near universality of the transition point, E_{c1} , with respect to k_f in a small range of R_M .

One can also determine the transition energy from the

point of intersection between the slopes fit to the two decay regimes, slow and fast. The slope intersection method depends on accurate fits for the two decay regimes and hence is subject to uncertainty. Also, as we see in Fig. 6 that the slopes are not constant in any of the decay regimes, and are continually changing, and therefore, the determined slope is an approximate average estimate. The fit in especially the fast decay regime seems highly uncertain, depending on the window of time chosen. Hence we do not pursue this method for determining the transition energy.

3.2 Transition identified by varying the initial field strength

Now we will examine the second kind of transition point, E_{c2} . This occurs when the initial magnetic field strength is lowered to a critical point below which the the field decays at a fast decay rate right from the beginning (i.e. the initial slow decay phase is now absent). We consider the evolution Eq. 16 for the large scale helicity and substitute $\langle \mathbf{j} \cdot \mathbf{b} \rangle$ in α_M (in the emf \mathcal{E} term) and $\langle \overline{\mathbf{J}} \cdot \overline{\mathbf{B}} \rangle$, with the corresponding two scale approximation of $k_f^2 \langle \mathbf{a} \cdot \mathbf{b} \rangle$ and $k_1^2 \langle \overline{\mathbf{A}} \cdot \overline{\mathbf{B}} \rangle$, respectively. We then get,

$$\frac{1}{2} \frac{\partial \langle \overline{\mathbf{A}} \cdot \overline{\mathbf{B}} \rangle}{\partial t} = \frac{1}{3\rho} k_f^2 \langle \mathbf{a} \cdot \mathbf{b} \rangle \tau \langle \overline{\mathbf{B}}^2 \rangle - \frac{u_{rms}}{3k_f} k_1^2 \langle \overline{\mathbf{A}} \cdot \overline{\mathbf{B}} \rangle - \eta k_1^2 \langle \overline{\mathbf{A}} \cdot \overline{\mathbf{B}} \rangle \quad (22)$$

Let us focus on the ideal limit of $\eta \rightarrow 0$, for which the total magnetic helicity is conserved at all times. Then, one can substitute for the small scale helicity in Eq. 22, $\langle \mathbf{a} \cdot \mathbf{b} \rangle = (\langle \overline{\mathbf{A}} \cdot \overline{\mathbf{B}} \rangle - \langle \overline{\mathbf{A}} \cdot \overline{\mathbf{B}} \rangle)$, where the total helicity ($\langle \overline{\mathbf{A}} \cdot \overline{\mathbf{B}} \rangle$) is conserved. Converting all the quantities to a dimensionless form, we get,

$$\frac{dM_1}{dt} + \frac{2}{3} M_1^2 - \frac{2}{3} M_1 (M_0 - (k_1/k_f)^2) = 0 \quad (23)$$

where $M_1 = \langle \overline{\mathbf{B}}^2 \rangle / (2M_{eq}) = k_1 \langle \overline{\mathbf{A}} \cdot \overline{\mathbf{B}} \rangle / (2M_{eq})$, $t/\tau = \tilde{t}$ and $M_0 = M_1(\tilde{t} = 0)$ is the normalised initial energy of the large scale helical field. Eq. 23 can now be solved to give,

$$M_1 = \frac{M_0 - (k_1/k_f)^2}{1 - \left(\frac{(k_1/k_f)^2 e^{(-2\tilde{t}(M_0 - (k_1/k_f)^2)/3)}}{M_0} \right)} \quad (24)$$

When $M_0 > (k_1/k_f)^2$, at late times $\tilde{t} \rightarrow \infty$, we have,

$$M_1 \rightarrow M_0 - (k_1/k_f)^2 \quad (25)$$

indicating that, the reduction in the field strength is by a finite amount. When $M_0 = (k_1/k_f)^2$, Eq. 23 becomes $dM_1/dt = -(2/3)M_1^2$ and hence $M_1 \rightarrow 0$ at late times.

And when $M_0 < (k_1/k_f)^2$, we obtain at late times when $\tilde{t} \rightarrow \infty$,

$$M_1 = M_0 \left(1 - (k_f/k_1)^2 M_0 \right) e^{(-2\tilde{t}((k_1/k_f)^2 - M_0)/3)} \quad (26)$$

which implies that the large scale field undergoes a rapid decay. Hence, $(k_1/k_f)^2$ forms a natural transition point, in the case of large R_M (or here in the ideal limit of $R_M \rightarrow \infty$), which determines when the LSHE will directly transit to rapid decay. This was emphasized in Paper I but without giving the above argument. The question arises how well this threshold, which holds in the ideal limit, obtains for more realistic R_M , both in the two scale model and the DNS. We first reconsider the two scale model.

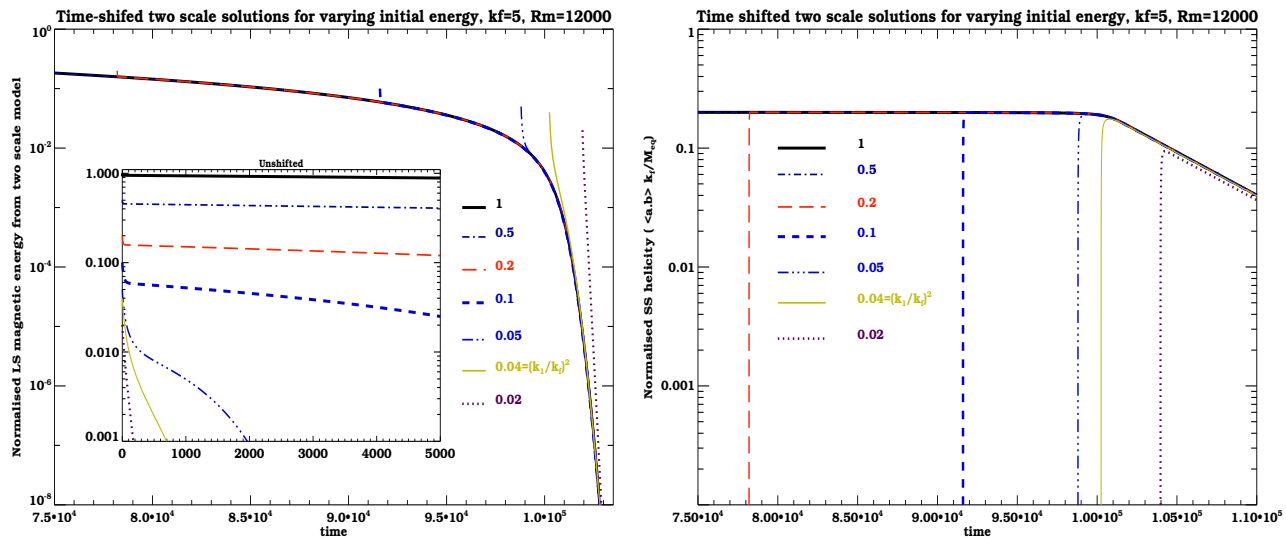


Figure 11. The decay curves from two scale model for fully helical large scale magnetic field for different initial strengths for $k_f = 5$ and $R_M = 12000$ are shown.

The left panel of Fig. 11, and Fig. 12, show the decay of fully helical large scale magnetic field for a set of decreasing initial field strengths for the two scale model. We have adopted $k_f = 5$ (Fig. 11) and $k_f = 20$ (Fig. 12), both with $R_M = 12000$. While the inset in the left panels of Fig. 11 and Fig. 12 show the evolution of large scale energy with decreasing initial strengths, the main plots show the curves starting with subequipartition strength, time-shifted to maximally coincide the $M_0 = 1$ evolution. The labels in the plot indicate the value of M_0 . The thick black curve is the case of $M_0 = 1$ (we will refer to this as the fiducial curve). In the curves beneath that of $M_0 = 1$, M_0 has been decreased to smaller and smaller values.

The right panel of Fig. 11 shows the evolution of the SSH. For stronger initial fields, SSH achieves a steady value and the resulting α_M is large enough to offset the turbulent diffusion. Then the large scale field decays initially at rate of the order resistive rate. When M_0 is below a critical value, the initial helicity in large scales is insufficient to generate a large enough small scale helicity, and α_M , by turbulent diffusion. In this case the SSH decays, and the LSHE decays fast due to turbulent diffusion (uncompensated by the α_M effect).

It can be seen from the right panel of Fig. 11 that the dash-dotted blue line starting with $M_0 = 0.05$ is the last to reach a steady state indicating the presence of resistive decay regime initially. For such smaller $M_0 \sim 0.04$ and below, the small scale helicity fails to rise to a steady state and subsequently decays indicating the absence of slow decay regime, which means that the large scale field directly starts decaying at a faster rate. This can be seen from the left panel of Fig. 11. Note that curves with M_0 above the threshold have sharp initial drop (as SSH builds up), but do not decrease in their energy significantly before joining the fiducial curve. On the other hand, the time-shifted purple dotted curve with $M_0 = 0.02$, which is below the threshold, drops by several orders of magnitude before joining the fiducial curve. Hence, we find that the transition point is close

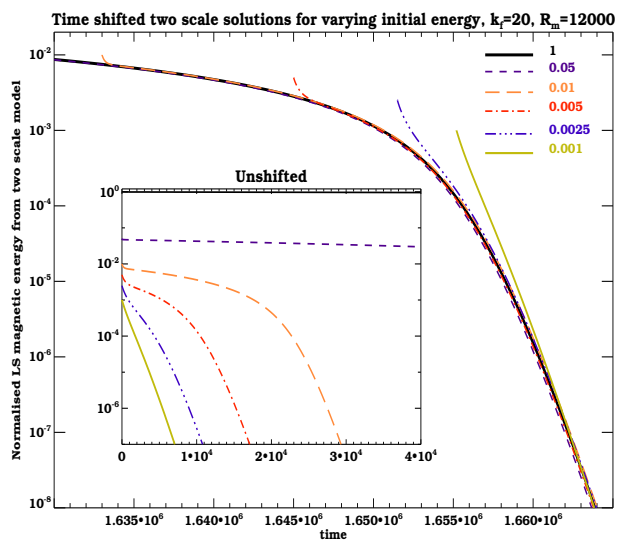


Figure 12. The decay curves from two scale model for fully helical large scale magnetic field with different initial strengths for $k_f = 20$ and $R_M = 12000$ are shown.

to the value of $(E_{c2}/M_{eq}) = (k_1/k_f)^2 = 0.04$ as expected from the work of Paper I and the Eq. 23 above.

Again the same exercise is repeated at $k_f = 20$. In the Fig. 12, the solid green curve starting with $M_0 = 0.001$, which is below the expected critical energy of $(k_1/k_f)^2$, is seen to drop in energy by few orders of magnitude before joining the fiducial curve. Hence in this case, we find the transition energy, $E_{c2} \sim 0.003 M_{eq}$, as is seen from the Fig. 12. This value of E_{c2} for the is again close to $(k_1/k_f)^2 M_{eq}$. Such large $R_M = 12000$ is however beyond the scope of current DNS. Thus in the DNS studies below, where R_M has a more modest value of ~ 100 , we may not expect to see such a clear evidence of E_{c2} . Nevertheless, we do expect to check the consistency with the two scale model and hence indirectly substantiate the results of Paper I.

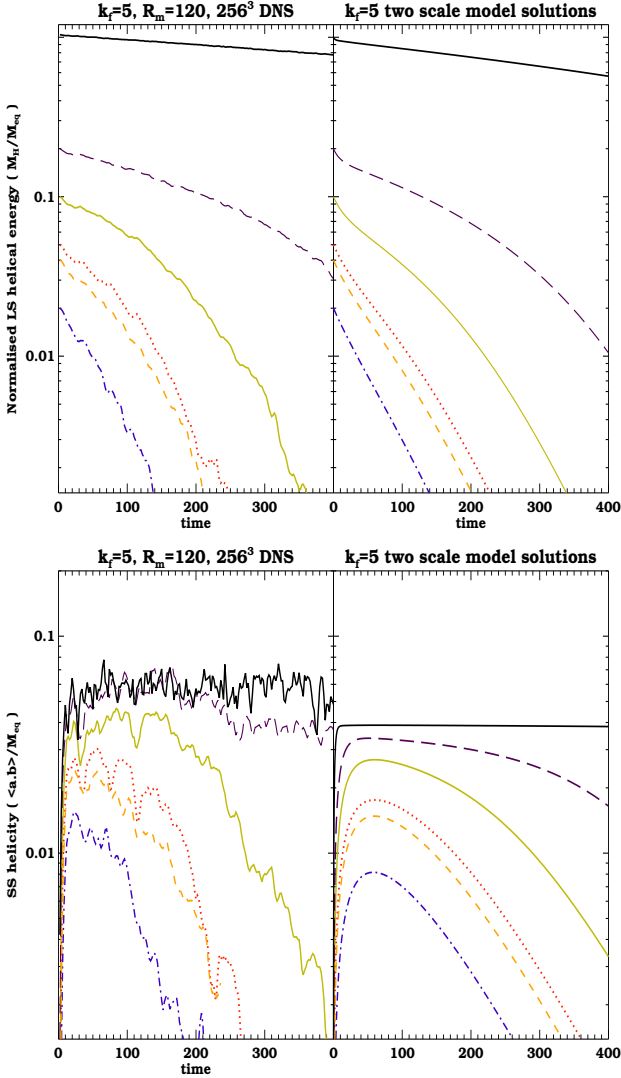


Figure 13. The decay curves for fully helical large scale magnetic field with different M_0 for $k_f = 5$ and $R_M = 120$, from DNS, are shown.

We have shown in Fig. 13, the results from the DNS runs G-K where the initial magnetic energy is lowered to smaller and smaller values compared to M_{eq} . In these set of simulations, we have fixed $k_f = 5$, $u_{rms} \sim 0.12$ and $\eta = 2 \times 10^{-4}$, and thus $R_M = 120$, while varying M_0 . The top left panel of Fig. 13 shows the time evolution of large scale magnetic energy in the DNS, while the top right panel the results from the corresponding two scale model. The time evolution of the SSH in the DNS and corresponding two scale model are respectively shown in the bottom left and right panels of Fig. 13.

A comparison between the DNS (left panel) and the 2-scale model (right panel) in Fig. 13, shows that there is a qualitative agreement between the two. For example, the slow decay rate of large scale energy of both are comparable, and so also are the amplitudes of the steady state small scale helicity. We also find that the average initial slopes (evaluated for the time period of $t=0$ to $t=100$) for all the runs G-K, listed in the Table 1, match closely with the es-

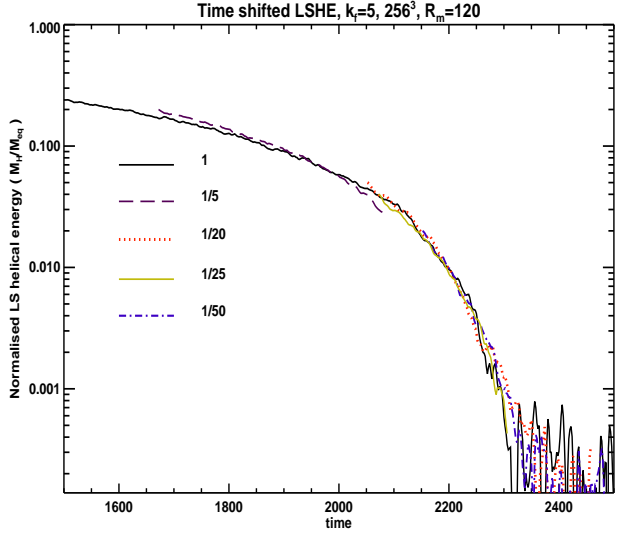


Figure 14. The time-shifted decay curve for fully helical large scale magnetic field for different sub-equipartition M_0 at $R_M \simeq 120$. This value of R_M does not meet the condition $3/R_M \ll (k_1/k_f)^2$ needed to identify the predicted transition (see text).

timate using Eq. 19, where the term in the denominator, $\langle \overline{\mathbf{B}^2} \rangle / 2M_{eq}$ is replaced with the value of M_0 .

In Fig. 14, we show the fiducial curve where $M_0 = 1$ is the solid black line. We also show the evolution curves starting with sub-equipartition energies, time-shifted to lie on the fiducial curve. As pointed out earlier, a clear energy transition value would be revealed if curves with M_0 below the threshold decrease in their energy significantly before joining the fiducial curve. The graph shows all the curves nearly falling together without any such drop in the initial energy which at face value means no clear identification of E_{c2} in the energy scale. However, from Eq. 19, it can be seen that the term $\eta/\eta_t = 3/R_M$ has to be sufficiently small compared to M_0 , to be able to discern the E_{c2} dependence on k_f , for the subsequent evolution. If we compare the two terms in the denominator of Eq. 19, then we require, $3/R_M \ll (k_1/k_f)^2$. Otherwise, η/η_t would become important before M_0 is lowered to $(k_1/k_f)^2$, and one cannot discern the influence of k_f on E_{c2} . With $k_f = 5$ and $R_M = 120$, $3/R_M = 0.025$ and $(k_1/k_f)^2 = 0.04$, thus the two terms are comparable. Hence, we seemingly need much higher R_M runs⁴ to be able to properly check the more conservative threshold of $E_{c2}/M_{eq} = (k_1/k_f)^2$.

Note that in Fig. 13, as M_0 is decreased, approaching E_{c2} from above, the subsequent decay seems to be at an increasingly higher rate. This can be understood from Eq. 19 (which applies only for $M_0 > E_{c2}$ since only in that regime does $\langle \mathbf{j} \cdot \mathbf{b} \rangle$ reach the steady state assumed by that equation.) For the curves with lower initial energy, the ratio,

⁴ On the other hand, in the context of E_{c1} , it is the term η/η_t which is responsible for the transition to faster decay phase. And we have seen that the transition energy E_{c1} depends on R_M , scaling as $R_M^{-1/2}$ from the two scale model solutions. Thus DNS with even a modest R_M can enable us to discern the transition energy, E_{c1} , which moreover agrees reasonably with that predicted by the corresponding two scale model solutions.

$\langle \overline{\mathbf{j}} \cdot \overline{\mathbf{b}} \rangle / \langle \overline{\mathbf{J}} \cdot \overline{\mathbf{B}} \rangle$ will be larger, thus leading to a higher multiple of the resistive decay rate. This can be understood from examining Fig. 14. Since the curves with lower M_0 , fall on the curve with $M_0 = 1$, later in time within the slow decay phase, they are expected to decay at an increasingly larger rate.

Overall we see a qualitative agreement between the DNS and the 2-scale model. This again indicates that the result of Paper I on the slow decay of helical magnetic fields which have $M_0 > (k_1/k_f)^2 M_{eq}$, seems reasonably consistent with the simulations that we have performed so far. Though higher resolution simulations with high R_M and small sub-equipartition initial fields are required to substantiate the above results.

3.3 Role of SSH in explaining $E_{c1} \neq E_{c2}$

In the distinct contexts of the previous two sections where we have identified the transition energies E_{c1} and E_{c2} we started with the SSH initially equal to zero. Here we discuss how the distinction between E_{c1} and E_{c2} can be traced to the distinct levels to which $\langle \overline{\mathbf{a}} \cdot \overline{\mathbf{b}} \rangle$ builds up in the two cases.

The first context (section 3.1) in which we have identified the the transition energy is the fiducial case of $M_0 = 1$, for which we found a k_f independent transition point E_{c1} . In this case, $\langle \overline{\mathbf{a}} \cdot \overline{\mathbf{b}} \rangle$ builds up to a nearly steady state value during much of the resistive slow decay phase of $\langle \overline{\mathbf{A}} \cdot \overline{\mathbf{B}} \rangle$ before the fast decay occurs. In contrast, for the second context (section 3.2) of varying M_0 , we found that when fast decay of the large scale field occurs right from the beginning, the helicity transferred from large scale to small scales never attains the aforementioned steady state value. The fast decay happens below a critical initial large scale helical energy value E_{c2} . If there is not enough initial helical large scale energy to supply the needed SSH, the large scale field decays fast. A source of SSH is crucial to explain the threshold of E_{c2} on k_f (Paper I).

To quantitatively study the importance of the role of SSH source in distinguishing E_{c1} and E_{c2} , we can ask if setting the initial SSH equal to the maximum steady state value of the case of section 3.1 (rather than allow it to grow from zero) and then vary the initial M_0 (as in the case of section 3.2) do we recover E_{c1} ?

Indeed, it is seen from Fig. 15, in the case of $k_f = 5$, $R_M = 12000$ and with the initial $\langle \overline{\mathbf{a}} \cdot \overline{\mathbf{b}} \rangle = (k_1/k_f^2) M_{eq}$, the two scale model solutions for varying M_0 fall together on the fiducial evolution curve for the context in section 3.1 For evolution starting at lower and lower energy values, the LSHE starts off initially with a flatter slope, but eventually joins the fiducial curve, which at that point in time is decaying at a much larger rate. The corresponding SSH quickly decays from the initial value of $(k_1/k_f^2) M_{eq}$ to the value on the fiducial curve at that point in time. Additionally, it can be seen from Fig. 16 that if SSH is set to a value, $0 < \langle \overline{\mathbf{a}} \cdot \overline{\mathbf{b}} \rangle < (k_1/k_f^2) M_{eq}$, then the two scale model solutions are similar to the second context, where SSH initially rises to attain the steady state value, and fails to do so when M_0 is at the threshold or below. This shows that the difference between the two contexts that led to $E_{c1} \neq E_{c2}$ obtains due to the difference in the value of SSH attained in the early transient phase of the evolution.

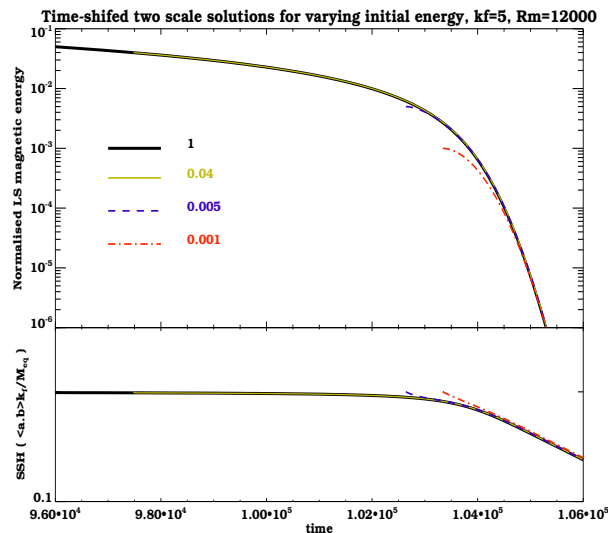


Figure 15. The two scale solutions for fully helical large scale magnetic field (in top panel) and SSH (in bottom panel) with different M_0 for $k_f = 5$ and $R_M = 12000$, where the initial SSH $\neq 0$, but is set to the value of $(k_1/k_f^2) M_{eq}$

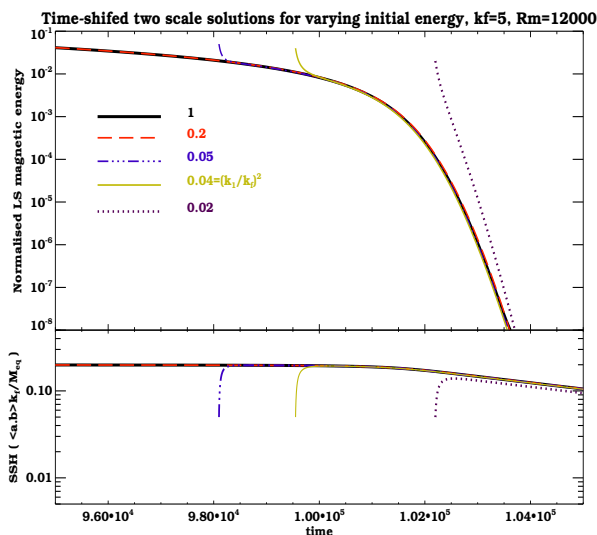


Figure 16. The two scale solutions for fully helical large scale magnetic field (in top panel) and SSH (in bottom panel) with different M_0 for $k_f = 5$ and $R_M = 12000$, where the initial SSH $\neq 0$, but is set to the value of $\langle \overline{\mathbf{a}} \cdot \overline{\mathbf{b}} \rangle k_f / M_{eq} = 0.2$

4 DISCUSSION AND CONCLUSIONS

The extent to which large scale fields survive turbulent diffusion in the absence of dynamo action via kinetic helicity or shear is important in assessing the plausibility of dynamo versus fossil field origin of large scale fields in astrophysical objects. Non-helical fields decay at the turbulent diffusion rate in the presence of non-helical turbulence, but large scale helical fields do not (Paper I). Here we have examined the survival of initially helical fields via direct numerical simulations (DNS), and compared the results with the basic two scale model of Paper I. Previous simulations have been done by Yousef et al. (2003) and Kemel et al. (2011).

In particular, we have examined the decay of large scale helical fields in more general settings by studying in detail the dependence on initial field strength, forcing wavenumber of the turbulence and also R_M . DNS takes into account the full set of MHD equations but is limited by computational power to modest R_M of order 100. On the other hand, the two scale model involves simplifying assumptions, of having only two scales and also invokes a closure approximation for the turbulent emf, but allows large R_M to be explored. Thus comparison will allow one to evaluate to what extent the two scale model can be trusted, and also then the possibility of extrapolating DNS to larger R_M . Overall, we find that there is good qualitative agreement between the predictions of two-scale theory and DNS.

For the case in which we start with an initial helical magnetic energy of sufficient strength, of order the equipartition value ($M_0 \sim 1$), the fields first exhibits a slow resistive decay. The decay rate steadily increases until the large scale helical energy falls to a few percent (3-5%) of the equipartition value. The resistive decay phase matches the predictions of the two scale model quite well. We can closely match the decay slope in this phase with Eq. 14. Moreover, we show that the assumption that α_K is much smaller than α_M , which was made in Paper I, holds true. This indicates that the basic picture of Paper I, particularly regarding the importance of a magnetic alpha, α_M , being generated by turbulent diffusion of the large scale helical field, and then itself acting to prevent the turbulent decay of the large scale field, is reasonably robust. This also indirectly supports the ideas behind the closure approximations used to derive the magnetic alpha.

Subsequently, there is a transition to fast decay phase, which can exceed even the turbulent decay rate predicted by a two scale theory. For this fiducial case of starting with equipartition energy, the threshold energy at which the transition occurs, E_{c1} , is independent of the forcing wavenumber k_f and R_M for the range of $R_M \sim 100$ explored. Meanwhile, the 2-scale model solutions at a much higher $R_M=12000$, do indicate a possible scaling of the transition energy $E_{c1} \propto R_M^{-1/2}$.

A different transition energy threshold E_{c2} arises for the case in which we seek the transition threshold at $t = 0$ below which the field decays at a fast rate right from the beginning. This scenario is more astrophysically relevant, since the feasibility of the existence of subequipartition strength initial fields is higher as compared to the fiducial case. In such a case, Paper I argues that when the large scale helical field energy is below a critical initial magnetic energy $E_{c2} \sim (k_1/k_f)^2 M_{eq}$, it decays rapidly at the turbulent diffusion rate. We have reconfirmed this estimate by solving the two scale model exactly in the ideal limit, and also solving it numerically for finite but very large R_M , much larger than possible by DNS. For the moderate $R_M \sim 100$ achievable by DNS (for DNS with large k_f), we have shown again that the DNS results are consistent with the 2-scale model. However, robustly identifying the transition energy E_{c2} predicted by the 2-scale model, requires the condition $3/R_M \ll (k_1/k_f)^2$ to be satisfied, and R_M is not sufficiently large in the simulations. Much higher R_M simulations would be required. At present we can only say that, from the overall consistency between DNS and 2-scale model even for case 1, we

do expect this later type of transition to obtain for high R_M cases.

Eventually it would be desirable to assess how the principles identified herein apply to more realistic conditions of astrophysical rotators to assess whether large scale fields in astrophysical rotators such as galaxies could result from post-processing of fossil helical fields without requiring a traditional in situ kinetic helicity. Real systems have shear, differential rotation, and stratification, all of which we have not considered here. We also considered all large scale quantities to be averaged over closed volumes in the present work, thereby eliminating helicity fluxes. It would be of interest for future work to consider the influence of helicity fluxes on the relative decay of helical and non-helical large scale fields. Finally we note that in real systems, there would in general be a combination of helical and non-helical fields and the results herein would apply to the helical fraction of the large scale magnetic energy.

ACKNOWLEDGMENTS

We thank Axel Brandenburg for useful discussions which helped to sharpen the arguments of this paper. We acknowledge the use of the high performance computing facility at IUCAA.

REFERENCES

- Beck R., 2012, SSRv, 166, 215
 Bhat P., Subramanian K., 2013, MNRAS, 429, 2469
 Blackman E. G., Brandenburg A., 2002, ApJ, 579, 359
 Blackman E. G., Field G. B., 2002, Physical Review Letters, 89, 265007
 Blackman E. G., Subramanian K., 2013, MNRAS, 429, 1398 (Paper I)
 Brandenburg A., 2003, Computational aspects of astrophysical MHD and turbulence. p. 269
 Brandenburg A., 2011, Pramana, 77, 67
 Brandenburg A., Subramanian K., 2005, PhR, 417, 1
 Clarke T. E., 2004, Journal of Korean Astronomical Society, 37, 337
 Clarke T. E., Kronberg P. P., Böhringer H., 2001, ApJ, 547, L111
 Field G. B., Blackman E. G., 2002, ApJ, 572, 685
 Fletcher A., 2010, in Kothes R., Landecker T. L., Willis A. G., eds, Astronomical Society of the Pacific Conference Series Vol. 438 of Astronomical Society of the Pacific Conference Series, Magnetic Fields in Nearby Galaxies. p. 197
 Govoni F., Feretti L., 2004, International Journal of Modern Physics D, 13, 1549
 Haugen N. E., Brandenburg A., Dobler W., 2004, PRE, 70, 016308
 Kazantsev A. P., 1967, JETP, 53, 1807
 Kemel K., Brandenburg A., Ji H., 2011, PRE, 84, 056407
 Kleorin N., Moss D., Rogachevskii I., Sokoloff D., 2000, A&A, 361, L5
 Krause F., Raedler K. H., 1980, Mean-field magnetohydrodynamics and dynamo theory
 Moffatt H. K., 1978, Magnetic field generation in electrically conducting fluids

- Pouquet A., Frisch U., Leorat J., 1976, *Journal of Fluid Mechanics*, 77, 321
- Rädler K.-H., Kleorin N., Rogachevskii I., 2003, *Geophysical and Astrophysical Fluid Dynamics*, 97, 249
- Ruzmaikin A. A., Sokolov D. D., Shukurov A. M., eds, 1988, *Magnetic fields of galaxies* Vol. 133 of *Astrophysics and Space Science Library*
- Schekochihin A. A., Cowley S. C., Taylor S. F., Maron J. L., McWilliams J. C., 2004, *ApJ*, 612, 276
- Subramanian K., 2002, *Bulletin of the Astronomical Society of India*, 30, 715
- Vogt C., Enßlin T. A., 2005, *A&A*, 434, 67
- Yousef T. A., Brandenburg A., Rüdiger G., 2003, *A&A*, 411, 321